Study of the sterile conk of *Inonotus obliquus* using ^{13}C CPMAS NMR and FTIR spectroscopies coupled with multivariate analysis

Gabriele Beltrame [a],[*], Ida Mattsson [b], Pia Damlin [c], Zenghua Han [d], Carita Kvarnström [c], Reko Leino [b], Baoru Yang [a]

[a] *Department of Biochemistry, Food Chemistry and Food Development, University of Turku, Itäinen Pitkäkatu 4, Turku, FI 20520, Finland*
[b] *Johan Gadolin Process Chemistry Centre, Laboratory of Molecular Science and Engineering, Åbo Akademi University, Turku, FI 20500, Finland*
[c] *Department of Chemistry, Turku University Centre for Materials and Surfaces (MatSurf), University of Turku, Turku, FI, 20014, Finland*
[d] *Institute of Microbiology, Heilongjiang Academy of Sciences, Zhaolin Street 68, Harbin, China*

ARTICLE INFO

ABSTRACT

The sterile conk caused by the infection of the basidiomycete *Inonotus obliquus* (Chaga) is an important source of bioactive compounds. However, its structure and biochemistry are only generally understood. Solid state ^{13}C NMR and FTIR spectroscopy have been utilized for the first time to investigate the sterile conk with non-invasive methods. The application of multivariate data analysis techniques and spectral distance algorithm to the obtained datasets showed clear distinction between the outer and inner layers of the sterile conk. Moreover, the sterile conk bark, compared to the inner layers, was spectroscopically more similar to wood tissues. The fungal tissue was proven to be concentrated below the bark. The similarity of the sterile conk inner layers to both decayed wood and hyphae of *I. obliquus* was shown by the multivariate data analysis of both spectra datasets. The spectroscopic data indicated lack of lignin degradation in the heart rot, except for demethoxylation, and a slight preference for hemicellulose degradation. Therefore, the results obtained suggest that the classification of *I. obliquus* as preferential lignin degrader (white-rot fungus) should be revised and clarified by further studies.

© 2022 The Authors. Published by Elsevier B.V.
This is an open access article under the CC BY license (http://creativecommons.org/licenses/by/4.0/)

1. Introduction

Fungi are receiving increasing attention from the research community as a source of bioactive compounds. Many species of interest are wood-decaying species, such as *Ganoderma lucidum, Fomitopsis pinicola*, and *Inonotus obliquus* [1]. Due to their ecological role, they are investigated also for biotechnological applications such as bioremediation and biopulping [2,3]. Wood-decaying fungi are classified into three categories: white, brown, and soft. The classification is based on morphological changes of the wood cell wall, the type of degraded cell wall component, and, to a lesser extent, the fungal taxonomy [4]. White-rot fungi degrade lignin, as well as cellulose and hemicelluloses, with a general preference for the first. There are two types of white-rot: "selective", favoring lignin degradation, and "simultaneous", with uniform degradation of all plant cell wall components. In the case of brown-rot, lignin is decomposed to a much lower extent, compared to cellulose and hemicelluloses. Polysaccharides are extensively hydrolyzed with slight alteration of the lignin matrix [4,5]. In soft-rot, degradation of polysaccharides is generally preferred, while lignin is degraded to a lesser extent, and, in general, demethylated. Wood decayed by brown-rot fungi becomes brittle, while soft-rot decay causes brash fractures and spongy texture. White-rot is caused by basidiomycetes and some ascomycetes, brown-rot is caused exclusively by basidiomycetes, and soft rot mainly by ascomycetes, although it has been suggested that some basidiomycetes can switch between white-rot and soft-rot types of degradation [4,5].

I. obliquus is a basidiomycetes of the family Hymenochetaceae (Hymenochetales) of circumboreal distribution, usually found above the 40th parallel north in United States, Canada, Scandinavia, North-Eastern Europe, Baltic countries, Siberia, and Northern China. It is an obligate parasite of the birch tree, classified as a white-rot fungi, producing yellow-brown resupinate basidiomes below the birch bark only once in the life cycle, at the death of the host. Its most common feature is a black cracked-shape protrusion from the bark, resulting from the interaction between the host and the parasite. *I. obliquus* penetrates the tree through open wounds and the sterile conk is formed at the site of the infection. This sterile conk, commonly called Chaga, is composed of sclero-

[*] Corresponding author.
E-mail address: gabbel@utu.fi (G. Beltrame).

tial hyphae and wood [6]. The utilization of the sterile conk of I. obliquus as traditional folk remedy goes back to the 16th century. Its extracts, in particular decoctions, have been used to treat a multitude of diseases, including gastro-intestinal and liver problems, tuberculosis and other infections and cancer [7]. Starting from ethnopharmacological evidence, multiple studies have focused on the bioactive components of *I. obliquus*, with a great deal of attention given to its polysaccharides. Over the years, the polysaccharides extracted from *I. obliquus* have been shown, among the available evidence, to scavenge radicals, to inhibit tumor growth *in vitro* and *in vivo*, to activate macrophages and promote cytokine production, and in general to exert immunomodulative activity [8].

Despite the attention given to its components and bioactivities, the sterile conk of *I. obliquus* is in itself poorly understood. It is formed at the inner periderm of the infection site, as the result of the pressure exercised by a wedge of fungal tissue on the outer bark. The pressure cracks open the bark, forming a protrusion of necrotic tissue [9]. The growth of the sterile conk (1–2 cm/year) is understood as the result of the compartmentalization attempt of the host, a model elaborated by Biggs [10]. The barrier of lignified wood tissue formed around the infection site is penetrated or circumvented annually [9–11]. At the same time, the mycelium, while exercising pressure towards the outer bark, colonizes the wood towards the sapwood and heartwood [11]. This is the generally accepted development model but has never been subjected to chemical investigation.

Different types of biomass have been studied with spectroscopic methods. Fourier Transform Infrared Spectroscopy (FTIR) is a rapid and non-invasive or non-disruptive technology. It has the advantages of easy sample preparation and measurement and wide applicability. FTIR provides information related to the presence or absence of specific functional groups, as well as the chemical structure of polymer materials. Shifts in the frequency of absorption bands and changes in relative band intensities indicate changes in the chemical structure or changes in the environment around the sample. FTIR has been applied to the analysis of polymeric substances, such as cellulose and hemicellulose [12,13], starch [14], and chitin [15]. It has also been used to obtain structural fingerprints of biomass. In particular, it has been applied to the study of the effects of fungal degradation on the chemical structure of wood [16]. Cross polarization magic angle spinning nuclear magnetic resonance spectroscopy (^{13}C CPMAS NMR) is another non-invasive technique, utilized for the analysis of solid samples. It is a common analytical method for the study of wood and wood components [17]. It has also been applied to the study of mushrooms [18] and chitins [15]. Importantly, it is a common technique for the study of fungal degradation of wood. This technique has been applied to the investigation of wood decay both by white-rot and brown-rot [19,20]. To increase further the value and potential of these techniques, multivariate statistical methods can been applied to FTIR and ^{13}C CPMAS spectroscopic data to identify similarities and differences between the samples and reduce the complexity of the dataset. The most common statistical method utilized with spectroscopic data for these purposes is principal component analysis (PCA), which has been applied to FTIR data obtained from wood of different geographical origin [21], from pretreated wood [22], from hemicelluloses [12], and fungal polysaccharides [23]. In addition, PCA has been applied to ^{13}C CPMAS datasets obtained from wood after thermal and brown- or soft-rot degradation [24], from wood of different geographical origin [17], from calcium alginates [25], and from dissolving pulp [26].

The objective of the present study was to investigate the nature of the sterile conk of *Inonotus obliquus* utilizing non-invasive methodologies and to verify the dated model proposed by Biggs [10]. The understanding of the starting material is becoming more relevant due to increasing attention to the sterile conk harvesting

after artificial inoculation in birch stands [27,28]. Moreover, a preference to the inner layers of the sterile conk as a resource of fungal polysaccharides has been reported but without a clear prior chemical justification [29]. At the same time, while the birch wood colonized and degraded by *I. obliquus* has been considered as a resource of polysaccharides, including fungal β-glucans [30], the nature of the decay caused by the fungus has not been previously investigated.

2. Materials and methods

2.1. Starting material

The stem section of a silver birch (*Betula pendula*) infected with *I. obliquus* and analyzed in this study was obtained from the municipality of Lieto (South-West Finland) after tree felling. A sterile conk of about 20 cm length, protruding from the same tree, about 10 cm above the upper stem cut, was collected as well. A commercial sample of ground sterile conk of *I. obliquus* (henceforth called Commercial Conk) was obtained from Eevia Oy (Seinäjoki, Finland).

Mycelium and aerial hyphae were obtained, for comparison purposes, from a strain of *I. obliquus,* previously isolated from a sterile conk. The strain was maintained on potato-dextrose-agar (PDA) slants at 30 °C and aerial hyphae were collected from the slants using a sterilized cutter and oven dried at 80 °C. The mycelium of *I. obliquus* was cultivated in 200 mL aqueous medium after seeding about 1 cm of agar slant. The cultivation medium contained (g/L): glucose 15; maltose 15; peptone 2; beef extract 1.3; MgSO$_4$·7 H$_2$O 1.5; KH$_2$PO$_4$ 3; vitamin B1 0.01. The medium was kept at 27 °C with a rotation speed of 140 rpm. At the end of the cultivation time, the mycelium was filtrated with a 30-mesh sieve, washed with double-distilled water, oven dried at 80 °C for 1 h, and ground in a mortar to about 3 mm particles [31].

2.2. FTIR

2.2.1. Sampling

The cut birch stem was sampled on the upper surface, starting from the bark and towards the heart rot, carving at approximately 1 cm of distance. Samples of outer bark, phloem, sapwood, and heart rot were collected with a clean chisel. Spectra were recorded from the samples as such by pressing them against a cleaned diamond ATR crystal using about 22 N of force with the sapphire force applicator. Clean crystal, with no force applied, was used as reference. A section of sterile conk was carved and small sections were sampled using a clean lancet. Sectioning was based on macroscopical differences among layers. Commercial Conk, ground mycelium and aerial hyphae were analyzed as such.

2.2.2. Data acquisition and pretreatment

FTIR spectra were recorded using a Bruker Vertex 70 spectrometer (deuterated tryglycerin sulfate detector (DTGS)) equipped with a single bounce (angle of incidence 45˚) attenuated total reflection (ATR) accessory (VideoMVP, Harrick), employing a diamond hemisphere with a crystal surface of 0.5 mm^2. Spectra were recorded in duplicate, sampling the region 1800–700 cm-1 with a spectral resolution of 2 cm^{-1}. For each spectrum, 128 scans were averaged. The ATR correction was performed with the OPUS software (Bruker Optik GmbH, Germany) and the data were exported. The spectral baseline was corrected and intensities were normalized to the most intense wavenumber (about 1080 cm^{-1}) using the Origin 2016 software. The data was then imported into RStudio [32] and the following steps were taken: The second derivatives of the spectra were calculated (package *signal*) and smoothed (Savitzky-Golay filter with 19 smoothing points). Positive values were replaced by 0 to preserve only peak information in the dataset and the signal

intensities were normalized to the range −1–0 (package *BBmisc*). After removal of wavenumbers with no variance, data were submitted to principal component analysis (PCA).

2.3. ^{13}C CPMAS NMR

2.3.1. Sampling

Different from FTIR, cross-polarization magical angle spinning ^{13}C NMR spectroscopy required up to 0.1 g of sample. Therefore, no precise layer sampling could be performed. Samples of outer bark, phloem, sapwood, and heart rot were collected with a clean chisel. Sections of the sterile conk were carved at approximately 1 cm of distance, sampling from the black bark towards the center of the proximal margin between the conk and the tree. All the carved samples and aerial hyphae samples were ground before ^{13}C CPMAS NMR analysis.

2.3.2. Data acquisition and pretreatment

Cross-polarization magical angle spinning ^{13}C NMR spectra were obtained with a Bruker AVANCE-III HD 400 MHz spectrometer. The powdered samples were spun at 14 kHz spin rate in a Bruker ^{1}H broadband double-resonance 4 mm CP MAS probe. The proton 90° high-power pulse was 2.9 μs and contact time 2 ms. The recovery delay time was set to 2 s and 10,000 scans were accumulated. The phase and baseline of the spectra were corrected with Bruker TopSpin software and exported. The ^{13}C CP-MAS spectra published by Santoni and coworkers [17] were used as reference for the baseline. ^{13}C CPMAS spectra were then binned (frequency ratio 10) and their intensities were normalized to 0–1 range. The crystallinity index of the sample cellulose was calculated from the ^{13}C CPMAS NMR spectra according to Wikberg and Maunu [33]. The methoxyl content of the lignin in wood and sterile conk samples was calculated using the calibration curve reported by Evstigneyev and coworkers [34]. Spectroscopic data were then imported in RStudio [32] and submitted to principal component analysis.

2.4. Principal component analysis and spectral distance

Principal component analysis was performed using the package *ChemoSpec*. The s-plot function was used to determine the most influencing variables of the first three principal components, which were represented by the extremes of the plot (Hanson B., personal communication). Therefore, frequencies situated below the 10th percentile or above the 90th percentile of the plot axes were selected and used for the interpretation of the data. The spectral distance between samples was computed with the same package and grouped by sample class comparison. For example, each distance between a mycelium spectrum and birch heart rot spectrum was labeled "Heart rot vs Mycelium". Kruskal-Wallis and pairwise Wilcoxon tests (package *car*) were used to assess significant differences in the averages of spectral distances among the sample classes, i.e., whether there was a significant difference between the average distances of "Heart rot vs Mycelium" and "Mycelium vs Sapwood".

3. Results and discussion

3.1. ^{13}C CPMAS NMR spectroscopy

The ^{13}C CPMAS NMR spectra of *I. obliquus* mycelium, aerial hyphae, and sterile conk samples, in addition to the spectra of phloem, sapwood and heart rot of infected birch, are reported in Fig. 1.

The spectra showed clear differences between the different classes of samples. The samples obtained from the sterile conk
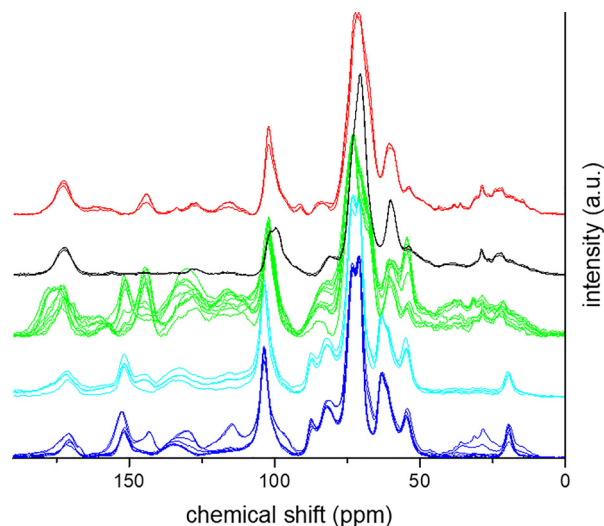

Fig. 1. Solid state 13C CPMAS spectra of mycelium (black), aerial hyphae (red), and sterile conk (green) of *I. obliquus* samples, together with birch phloem (blue), sapwood (blue), and heart rot (cyan) samples. Commercial Conk sample is highlighted in dark green.

clearly differed from the birch wood samples, in particular in the spectral area 120–180 ppm. The carbon distribution of the samples, crystallinity index, and the lignin methoxyl content were calculated from the spectroscopical data and are reported in Table 1.

Samples obtained from the sterile conk had the highest amount of aromatic carbon and, together with mycelium and hyphae samples, of carbonyl carbon. The undecayed sapwood samples had the highest content of carbohydrate backbone (60–90 ppm) carbon and, together with heart rot, of anomeric carbon. The sterile conk samples had the lowest amounts of carbohydrate backbone carbon. The spectroscopical data were submitted to principal component analysis (PCA) for better visualization of the chemical similarities and differences among the samples. The score and loading plots resulting from the analysis are shown in Fig. 2.

The PC1 vs PC2 plot, which already represented 70% of the data variance, showed that PC1 (48% of total variance) distinguished the sterile conk samples from the rest of the dataset. The second principal component, on the other hand, grouped the cluster made of sapwood, phloem and heart rot samples with only certain samples obtained from the sterile conk, while the other sterile conk samples grouped on the other side of the component with the cluster of mycelium and aerial hyphae samples. The sterile conk samples that grouped with, and were therefore more similar to, birch wood and cultivated fungal tissue, were the yellow surface and the bark samples, respectively. In the PC2vsPC3 plot (Fig. 2), the third principal component grouped the sterile conk bark samples with the mycelium and aerial hyphae samples, indicating the presence of spectral similarities. The loading plots of PC1, PC2, and PC3, indicating which chemical shifts were responsible for the similarities observed in the score plots, are reported as well in Fig. 2. Noticeably, most of the significant chemical shifts of PC1 have negative loadings, indicating that the discrimination of the sterile conk samples from the other samples was based on the frequencies of the latter, except for the signal at 128 ppm. The assignments of the 10% most important frequencies of the PCA loadings are reported in Table 2.

The PCA model was mainly affected by the spectral region of the carbonyl and aromatic signals (170–110 ppm) and by the polysaccharide structure signals (110–60 ppm). The chemical shifts at around 128 ppm, assigned to the unsubstituted carbon of aromatic moiety, positively correlated with the sterile conk sam-

Table 1
Cristallinity index, methoxyl content of sample lignin and carbon distribution of the samples, obtained from ^{13}C CPMAS data.

	CrI (%)*	Lignin methoxyl content (lignin%)#	Carbon distribution (area%)					
			Alkyl/Acetyl 5–45 ppm	Methoxyl 50–60 ppm	Carbohydrate backbone 60–90 ppm	Carbohydrate anomeric 95–110 ppm	Aromatic 110–160 ppm	Carbonyl 160–180 ppm
Phloem	31.89 ± 1.68 b	3.99 ± 0.02 a	8.51 ± 2.25 b	5.84 ± 0.86 a,c	49.46 ± 0.01 c	13.02 ± 0.51 b	19.62 ± 0.81 a,b	3.54 ± 0.08 b
Sapwood	40.61 ± 1.91 a	4.24 ± 0.05 b	3.43 ± 0.34 c	5.42 ± 0.17 a,c	62.58 ± 1.50 d	15.05 ± 0.39 c	10.96 ± 1.98 d	2.55 ± 0.19 b
Heart Rot	41.46 ± 0.75 a	4.08 ± 0.05 a	4.51 ± 0.90 c	5.93 ± 0.12 a	55.52 ± 3.46 b	14.38 ± 0.25 c	16.16 ± 2.54 b	3.49 ± 0.25 b
Conk Bark	40.50 ± 2.50 a	4.02 ± 0.03 a	13.29 ± 0.90 a	6.13 ± 0.41 a	39.47 ± 1.81 a	10.43 ± 0.37 a	23.71 ± 2.93 a	6.96 ± 1.60 a
Conk Surface	35.25 ± 1.66 b	3.90 ± 0.07 a	9.88 ± 1.81 b	3.47 ± 1.24 b	40.25 ± 1.22 a	13.01 ± 0.68 b	24.63 ± 3.25 a	8.76 ± 1.22 a
Mycelium	n.a.	n.a.	15.12 ± 0.80 a	5.82 ± 0.21 a,c	57.74 ± 0.48 b	10.03 ± 0.10 a	4.25 ± 0.49 c	7.04 ± 0.11 a
Aerial Hyphae	n.a.	n.a.	12.78 ± 0.83 a	4.26 ± 0.30 b,c	56.84 ± 1.02 b	10.44 ± 0.47 a	8.32 ± 0.90 c,d	7.36 ± 0.44 a

Different letters mark significant difference ($p < 0.05$).
* Calculated with the method reported in [33].
# Calculated from the calibration curve reported in [34].

ples. Signals that are typically assigned to lignin, such as those at 152 ppm and 143 ppm [17,24,33], correlated as well with the sterile conk. However, these signals are produced by etherified and free hydroxyl positions of aromatic units, therefore phenolic compounds could also be ascribed for these signals [20]. The signal around 104 ppm, assigned to β-anomeric polymers (i.e., cellulose) was relevant for both PC1 and PC2, but while for the earlier its loading was almost zero, for the latter the loading was negative. Therefore, the signal distinguished birch wood and sterile conk bark samples from the others (Fig. 2). The α-anomeric signal, on the other hand, had a positive loading on both PC1 and PC2, therefore correlating with the sterile conk surface. Likewise, the PC1 and PC2 loadings of O-substituted C6 signal (69 ppm) correlated with the sterile conk surface samples. However, the loadings were determinant only for PC2. This signal can be observed in fungal polysaccharides such as β-glucans, α-mannans, and α-galactans [35,36]. The β-glucans and α-galactans were identified in the extracts of mycelium and sterile conk of *I. obliquus* [30] and are among the main compounds of interest produced by this fungi. The signals assigned to C4 of crystalline and amorphous cellulose (88 and 82 ppm, respectively) correlated with the birch wood samples and with the sterile conk bark. This observation is supported by the calculation of the cellulose crystallinity index, which significantly decreased only in the sterile conk surface samples (Table 1). The backbone polysaccharide signals, in particular at 71 ppm (C2, C3, and C5 of cellulose and hemicellulose), correlated with birch wood and sterile conk bark, highlighting their higher relative intensity compared to the other samples, except at 60 ppm, which correlated specifically with the sterile conk yellow surface. The latter signal could be assigned to C6 of α-glucans, such as glycogen, or β-(1,3)-glucans. The chemical shifts at around 172 ppm had a clear correlation with the sterile conk surface samples. These signals could be however assigned to the carbonyl of both ester and amide [17,18,37]. The extracted and normalized ^{13}C CPMAS NMR spectral area 190–140 ppm of mycelium, aerial hyphae, sterile conk, and heart rot samples is reported in Fig. 3.

All the spectra showed the peak around 143 ppm, which determined the position of the sterile conk surface samples on PC3, and the peak around 152 ppm, which correlated with the sterile conk bark (Fig. 2 and Table 2). Moreover, the sterile conk surface and aerial hyphae samples showed peaks at around 157, 159, 161, and 165 ppm. These peaks could be assigned to compounds of the stirylpyrone class [38,39], which have been isolated from sterile conk and mycelium of *I. obliquus* and from other *Inonotus* spp. and have shown multiple biological activities, including anti-oxidant, citotoxic and anti-inflammatory [40,41]. The sterile conk samples showed a strong peak at 173.6 ppm, while this peak shifted to 172.6 ppm in mycelium and aerial hyphae samples and to 171.9 ppm in the birch heart rot samples (close to the 171.1 ppm signal of sapwood, not shown). This peak, which was ascribable to acetyl or amide carbonyl, overlapped with the signal at 178 ppm, which, on the other hand, was ascribable to the carboxylic moiety. Noticeably, the carboxyl group signal was the strongest in the sterile conk bark samples (Fig. 3).

3.2. FTIR

The FTIR spectra collected from the sterile conk, mycelium, and aerial hyphae of *I. obliquus* and from the sapwood and heart rot of birch infected by *I. obliquus* are reported in Fig. 4a.

The present study focused on the mid IR region, 1800–750 cm^{-1}. The samples showed clear differences in the wavenumber intensities after ATR correction and normalization. The undecayed birch samples (light blue) showed the typical absorbance bands in the 1640–1595 cm^{-1} region ascribable to absorbed moisture and lignin skeletal vibrations. This typical pattern was absent in the
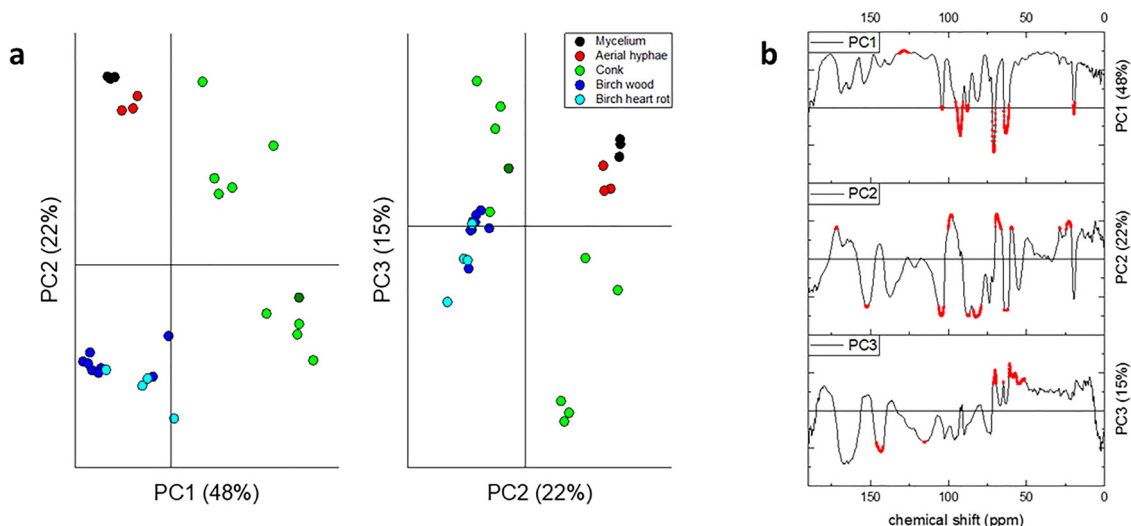
Fig. 2. Score (a) and loading (b) plots of the PCA of the ^{13}C CPMAS spectra dataset. Commercial Conk sample is highlighted in dark green.

Table 2
Loading assignments of the PCA model obtained from ^{13}C CPMAS data.

Principal component	Chemical shift (ppm)	Position on principal component	Structural assignment*
PC2	172	+	C=O Ester, amide
PC2	152	−	C=C Etherified position aromatic unit
PC3	143	−	C=C Free hydroxyl position aromatic unit
PC1	128	+	Unsubstituted aromatic C=C
PC3	115	−	Unsubstituted aromatic C=C
PC1, PC2	104	−	β-glycosydic linkage
PC2	99	+	α-glycosydic linkage
PC1, PC2	88	−	C4 crystalline cellulose
PC2	82	−	C4 amorphous cellulose, C4 hemicellulose
PC1, PC3	71	-, +	C2, C3, C5 cellulose, hemicellulose
PC2	69	+	C6 O-substituted
PC3	65	+	C6 cellulose, hemicellulose
PC1	63	−	
PC2	62	−	
PC3	61	+	
PC2	60	+	
PC3	57	+	O**C**H
PC2	29, 23	+	Saturated carbon chain (lipids, proteins)
PC1	19	−	CO**C**H3

* Refs. [17,33].

sterile conk samples (green), while strong absorbance bands due to aromatic vibrations were present. On the other hand, the spectra recorded from cultivated *I. obliquus* (black and red for mycelium and aerial hyphae, respectively) showed the clear protein signal at 1639 cm^{-1}. A detailed study of the frequencies of the absorption bands of the dataset was performed using the second derivate of the obtained FTIR spectra. The intensities $(0 - -1)$ of the second derivatives are reported in Fig. 4b, coupled with a hierarchical cluster analysis. While the indication of the wavenumbers determining the clustering is absent from Fig. 4b, groupings in the dataset were highlighted, indicating similarities and differences among the analyzed samples. The function used the default Euclidean distance. The birch wood (birch softwood) samples clustered separately from the rest of the dataset. In the rest of the samples, birch wood (phloem) and some sterile conk samples (layer 2, Supplementary Fig. 1) separated from the others, which on the other hand separated into two groups, one containing sterile conk (layer 1) and heart rot samples, the other containing sterile conk, aerial hyphae, and mycelium samples. Therefore, hierarchical cluster analysis of the second derivatives indicated that some sterile conk sampled layers were more similar to cultivated *I. obliquus* than to wood. These similarities were further investigated with the principal component analysis, which allowed also the identification of the most important wavenumbers influencing the separation of the samples. The resulting score and loading plots are reported in Fig. 5a,b. The numbering of the sterile conk sample followed the numbering of the different layers identified visually in the sampled section (Supplementary Fig. 1).

The PC1vsPC2 plot represented in total 82% of the dataset variance, with PC1 representing already 65%. The PCA clearly showed the separation of the birch wood samples from the rest of the data set, which was marked by PC1. In Fig. 5a, samples from cultivated *I. obliquus* and sterile conk samples are situated opposite to birch wood samples. Stem phloem samples grouped together with the sterile conk samples layer 2, close to the middle of PC1. Not only the spectra of these samples were similar, but also layer 2 of the sterile conk section was macroscopically similar to birch phloem. The birch sample closest to the sterile conk samples in Fig. 5a was taken from the birch bark, while the adjacent sterile conk sample was taken from the outer black bark. In the same plot, heart rot and the Commercial Conk sample grouped together and layers 6 and 7 of sterile conk were close to this group. The third principal component represented only 8% of the total variance, adding therefore little information. However, in the PC1 vs PC3 plot (Fig. 5a)
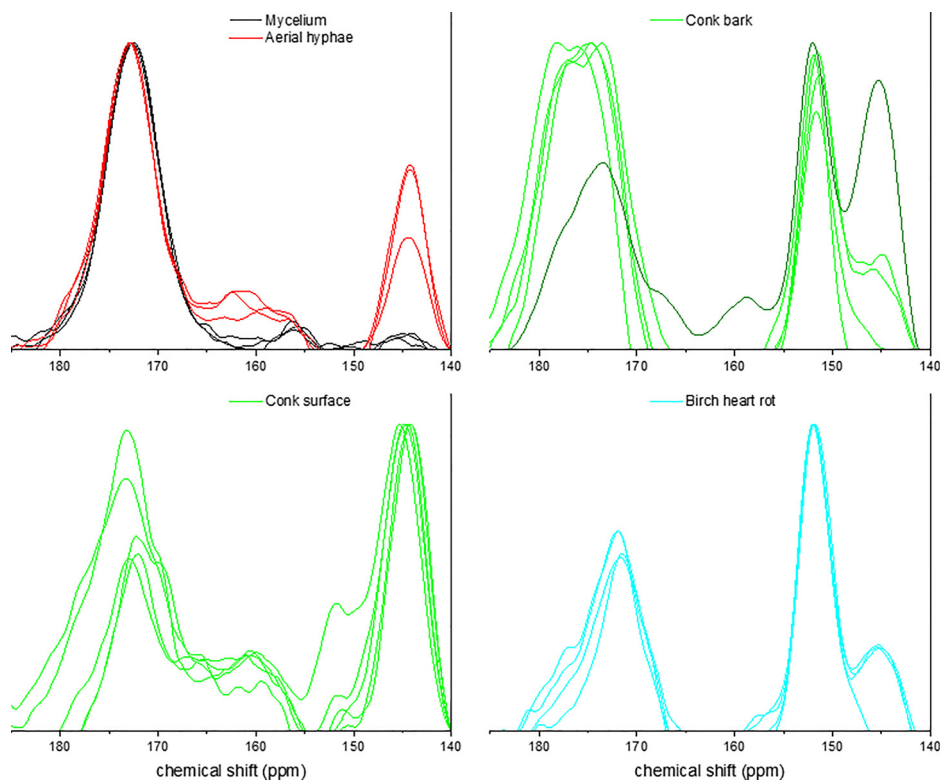
Fig. 3. Focus on the 140–185 ppm region of the solid state 13C CPMAS spectra of mycelium, aerial hyphae, and sterile conk of *I. obliquus*. Spectra were smoothed and normalized. Commercial Conk sample is highlighted in dark green.
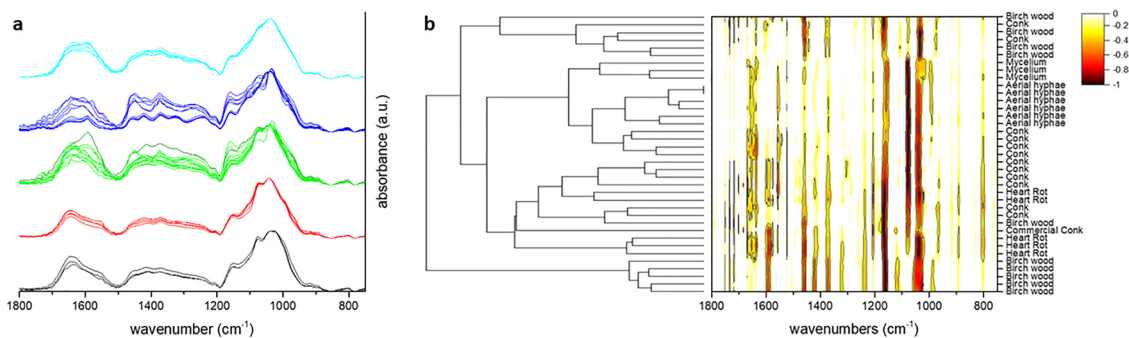

Fig. 4. (a) ATR-FTIR spectra of mycelium (black), aerial hyphae (red), and sterile conk (green) of *I. obliquus* samples, together with birch phloem (blue), sapwood (blue), and heart rot (cyan) samples; Commercial Conk sample is highlighted in dark green. (b) HCA of the second derivative of the ATR-FTIR dataset.

the grouping of aerial hyphae, mycelium, and sterile conk samples (layers 3, 4, and 5, Supplementary Fig. 1) was clearly visible. These samples had however scores of PC3 similar to the birch wood samples. The loading plots reporting the most determinant variables for the position of the samples on PC1, PC2, and PC3 discussed before are reported in Fig. 5b. The position of the birch wood samples was determined by the frequencies 1634, 1551, and 1082 cm^{-1}, which are ascribable to O-H, aromatic C=C, and C-O bonds, respectively. The peculiarity of the first two was noticed also in the visual comparison of the FTIR spectra (Fig. 4a). The cluster made by the heart rot, phloem, and sterile conk bark samples on PC2 was determined by the wavenumbers 1610, 1443, and 1385 cm^{-1}, which could be assigned to the vibrations of aromatic C=C, COOR, and C-H bonds, respectively. The position of the sterile conk samples in the lower left quadrant of PC1vsPC2 was determined by the wavenumbers 1113 (C-O-C), 1053 (C-O), and 976 (C-O) cm^{-1}. The position of mycelium and aerial hyphae samples was deter-

mined mainly by amide (1589 cm^{-1}) and C-O-C (1161 cm^{-1}) bands (Table 3).

The obtained model discriminated the undecayed birch wood from the rest of the dataset. A second PCA model was computed excluding birch bark, phloem (including the samples found in the sterile conk), and sapwood, to further assess the spectroscopical similarities between the different layers of the sterile conk, decayed wood and cultivated *I. obliquus*. Score and loading plots of the second model are reported in Fig. 5c,d, respectively. The first principal component (37% of total variance) discriminated between the heart rot and cultivated *I. obliquus* samples. Noticeably, the position of the sterile conk samples was not homogenous, some layers positioned closer to mycelium and aerial hyphae samples, while others were closer to heart rot. Particularly, layers 3, 4, and 5 grouped together with cultivated samples. On the other hand, the sterile conk layer 1 (black bark) grouped together with heart rot samples. The remaining layers were close to the heart rot sam-
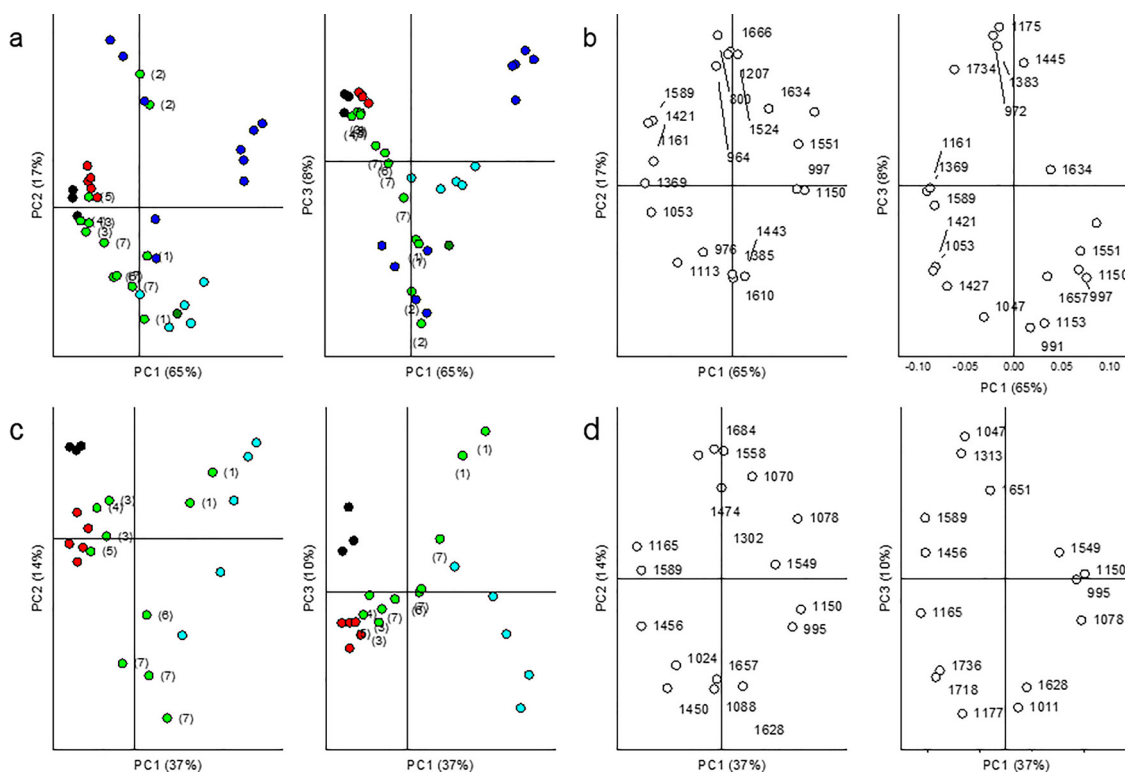
Fig. 5. Score (a) and loading (b) plot of the PCA of the whole ATR-FTIR spectra dataset; score (c) and loading (d) plot of the PCA of the ATR-FTIR spectra dataset without undecayed samples. Commercial Conk sample is highlighted in dark green.

Table 3
Loading assignments of the PCA model obtained from ATR-FTIR data.

PC1			PC2			PC3		
wavenumber	position	assignment	wavenumber	position	assignment	wavenumber	position	assignment
				Model from whole dataset				
1634	+	O-H	1666	+	amide	1734	+	COOR
1589	−	amide	1610	−	C=C aromatic	1657	-	amide
1551	+	C=C aromatic	1524	+	C=C aromatic	1445	+	COOR
1421	−	C-H	1443	−	COOR	1427	-	C-H
1369	−	C-H	1385	−	C-H	1383	+	C-H
1161	−	C-O-C	1207	+	C-O	1175	+	C-O-C
1150	+	C-O-C	1113	−	C-O-C	1153	-	C-O-C
1082	+	C-O	976	−	C-O	1047	-	C-O
1053	−	C-O	964	+	C-O	991	-	C-O
997	+	C-O	800	+	α-linkage	972	+	C-O
			Model from dataset without undecayed samples					
1589	−	amide	1684	+	ketone	1736	-	COOR
1549	+	C=C aromatic	1657	−	amide	1718	-	COOH
1456	−	C-H	1628	−	O-H	1651	+	amide
1165	−	C-O-C	1558	+	amide	1628	-	O-H
1150	+	C-O-C	1474	+	C-H	1313	+	C-H
1078	+	C-O	1450	−	C-H	1177	-	C-O-C
995	+	C-O	1302	+	C-O	1047	+	C-O
			1088	−	C-O	1011	-	C-O
			1070	+	C-O			
			1024	−	C-O			

ples but about at the center of PC1. Their position would suggest that these samples were spectroscopically similar to both the birch heart rot and cultivated *I. obliquus*. The second principal component (14% of total variance) grouped together these samples, although the cluster was less clear, compared to the other two. Interestingly, on PC2 the sterile conk samples 3, 4, and 5 positioned closer to aerial hyphae than to mycelium (Fig. 5c). The PC1 vs PC2 loading plot (Fig. 5d), the clustering of the aforementioned sterile conk samples and aerial hyphae was determined by the

wavenumbers 1589 (PC1), 1456 (PC1), 1450 (PC2), 1165 (PC1), and 1024 (PC2) cm^{-1}. These wavenumbers were assigned to the amide group and C-H, C-O-C, and C-O bonds, respectively. On the other hand, the positions of birch heart rot and sterile conk remaining layers on PC1 were determined by the wavenumbers 1549, 1150, 1078, and 995 cm^{-1}, which were ascribable to aromatic C=C, C-O-C, and C-O, respectively (Table 3). Particularly, the wavenumbers 1165 and 1024 cm^{-1} can be assigned to fungal glucans, while the wavenumbers 1150 and 1068 cm^{-1} can be assigned to hemi-
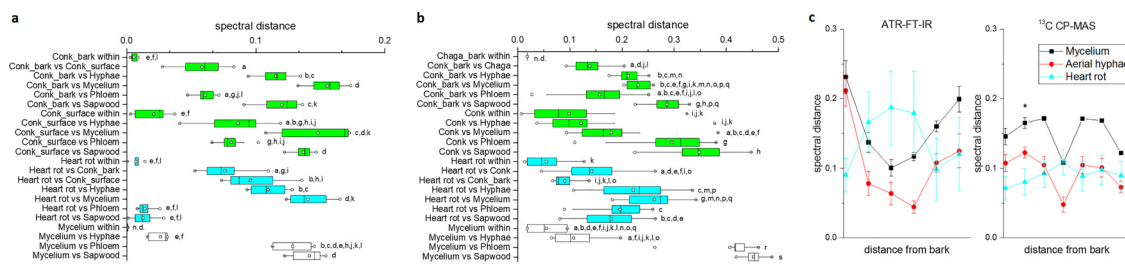
Fig. 6. Boxplot of the spectral distances between sample classes in the 13C CPMAS (a) and ATR-FTIR (b) spectra dataset. Different letters mark significant difference ($p < 0.05$). (c) Spectral distance of sterile conk samples from aerial hyphae, mycelium, and birch heart rot in function of the sampling distance from the bark. *Sample absent from ATR-FTIR dataset.

celluloses [13,42,43]. Infrared spectroscopy, differently from NMR, clearly grouped the inner sterile conk layers and aerial hyphae according to the amide signal. This indicated higher abundance of fungal tissue below the bark but suggests also higher presence of polymers of interest, as the layers correlated with fungal glucan signals, in accordance with ^{13}C CPMAS data.

3.3. Spectral distance

For both the ^{13}C CPMAS NMR and FTIR datasets, the Pearson distances between each pair of spectra were computed using the *sampleDist* function of the *ChemoSpecUtils* package. The Pearson distance has a range 0–1: samples with distance closer to zero have high similarity, while a distance of zero indicates identity of the two spectra. The obtained matrixes were divided by sample class comparison. The classes "Conk_bark" and "Conk_surface" were used in the data analysis of the ^{13}C CPMAS NMR data due to the separation of the samples in the PCA, while the labels "Conk_bark" and "Conk" were used for the FTIR dataset. Phloem and sapwood were considered as two separated classes. Comparison within the same class was considered as well and was labeled as "within". Our investigation focused on the comparisons relevant to the investigation of the sterile conk of *I. obliquus*. The boxplot of the sample class comparisons are reported in Fig. 6. The skewness, kurtosis, and variance of the spectral distance comparisons are reported in Supplementary Table 1.

Different observations could be made regarding the spectral distance, and hence the similarity, of the samples taken from bark and layers of sterile conk with birch heart rot, birch undecayed sapwood, phloem, and cultivated *I. obliquus*. The boxplot of the distances measured with the ^{13}C CPMAS NMR dataset is reported in Fig. 6a. The spectra of the sterile conk bark resulted equally distant from birch heart rot and from the sterile conk surface. The sterile conk surface resulted, however, closer to the sterile conk bark than to the decayed wood and to the cultivated mycelium. On the other hand, there was no significant difference in the distances between the sterile conk surface and its black bark and between the sterile conk surface and aerial hyphae. Likewise, the distance between the sterile conk surface and the heart rot was equivalent to the distance between sterile conk surface and aerial hyphae. At the same time, the spectra of the sterile conk surface was significantly more similar to aerial hyphae than to mycelium. Compared to the NMR spectra, different observations could be drawn from the distances observed between the FTIR spectra (Fig. 6b). Infrared spectroscopy indicated equal distances between the sterile conk bark, inner layers (3–7), and the heart rot. At the same time, the distance of the sterile conk layer from the black bark was equivalent to the distance from the mycelium and the aerial hyphae. However, the FTIR dataset indicated, contrary to NMR spectroscopy, a higher similarity of the sterile conk layers with aerial hyphae than to heart rot, while confirmed the higher similarity of the sterile conk internal layers to the aerial hyphae, rather than to mycelium.

Since both datasets were obtained from samples carved from the bark towards the center of the sterile conk, it was possible to report the trend of the spectral distances of the samples from mycelium, aerial hyphae, and heart rot, in relation to the sampling distance (Fig. 6c). A decreasing distance from cultivated *I. obliquus* in the samples can be noticed, followed by an increase, moving further from the bark. The samples taken from the surface of the sterile conk for ^{13}C CPMAS NMR were taken at about 1 cm of distance. Therefore, the reason of the sudden decrease of the spectral distance could be merely due to the sampling of a mycelium granule in the amorphous structure [6]. The sampling for FTIR followed visual differences in the layers and the samples taken were below the black bark (except for the black-brown layer right below, which was analyzed only by NMR spectroscopy). The observed phloem was excluded from Fig. 6c. The similarity of the outer layers with the aerial hyphae samples would indicate the presence of packed hyphae right below the bark, which in turn, as we have shown, was spectroscopically closer to birch wood. The hyphal colonization would be then sparser in the inner layers of the sterile conk. There is no difference in the distance between these layers and hyphae or heart rot. This was observed also in the PCA analysis (Fig. 5c). While this has already been macroscopically described [6], there are, to the best of our knowledge, no reports on the microscopical structure of the sterile conk of *I. obliquus*. Our findings would confirm the model of conk formation proposed by Biggs [10], which has never been chemically verified with the sterile conk of *I. obliquus*. Despite the importance of this nutraceutical resource, the research on its growth and development is lacking.

Outer and inner sections of the sterile conk of *I. obliquus* have been considered distinct resources of biactive compounds only in a limited amounts of studies: Wold considered the inner layers as better source of polysacchardes [29] and Nakajima observed higher anti-oxidant activity in inner layer extracts [44]. Recently, Kim and coworkers found differences in the presence of bioactive terpenoids between inner and outer layers [45]. Our findings could explain these differences. Moreover, the increased interest in the cultivation of the sterile conk with birch stands for industrial purposes gives higher importance to the understanding of its development and of the production of its bioactive compounds.

The Commercial Conk sample has been included in the calculation of the spectral distances in the datasets. Therefore, it was possible to assess the spectral distance between the commercial sample and the different classes of samples studied in this work. The results are reported in Supplementary Fig. 4. In both FTIR and ^{13}C CPMAS NMR datasets, the farthest sample class was the mycelium, followed by aerial hyphae. In the first dataset, there were no significant differences in the distances from mycelium, aerial hyphae, and phloem. The sample classes closer to Commercial Conk were sterile conk bark and heart rot, with no significant differences. The inner layers of sterile conk and the sapwood were farther from Commercial Conk, however, without significant difference from sterile conk bark and heart rot. Solid state NMR spec-

troscopy showed a different trend. Aerial hyphae samples were significantly closer to Commercial Conk, compared to mycelium, but the distance was the same as between Commercial Conk and sapwood. Heart rot, phloem, and sterile conk surface were closer but had statistically the same distance. The bark sterile conk had the shortest distance from the sample. This information is relevant because it raises the question of the relative amounts of sterile conk bark and inner layers that would be present in Chaga products available from the market. Our results have shown the presence of fungal tissues mainly in the inner layers of the sterile conk. Therefore, bioactive compounds such as the β-glucans are expected to be present in higher amounts in the inner layers, where their chemical fingerprints have been observed. However, the amount of inner layers in the products would be influenced by factors such as dimensions (and therefore the age) of the sterile conk collected from the forest. Further studies and the quantification of specific markers of fungal colonization, such as fungal metabolites, would be required to establish a quantitative relationship between the presence of bioactive compounds and the amount of sterile conk bark in the commercial product.

3.4. Effect of I. obliquus *degradation on birch wood*

The effect of *I. obliquus* degradation on lignocellulose biomass was studied by Xu and coworkers [46]. However, the study was performed in submerged cultivation conditions using different straws as the lignocellulose supplement. In our study, the comparison between degraded and undegraded wood was performed analyzing the heart rot caused by the fungus in a wild birch tree. In the FTIR spectra, the clearest effect of *I. obliquus* colonization was the disappearance of the 1730 cm^{-1} band (COOR), which could be connected to the degradation of hemicelluloses [47], and the increase in intensity of the 1590 cm^{-1} band, which was ascribable to the deposition of phenolic compounds by the birch tissues. The increase in the intensity of this band would contradict the previous report and the classification of *I. obliquus* as a white-rot fungus, due to its production of ligninolytic enzymes [46]. The research on the topic is scant. However, experiments on wood colonization of *Inonotus hispidus* have shown that, while the fungal host deposited polyphenolic compounds, the hyphae avoided the physical barriers and the deposits of toxic substances [5]. These findings were also observed in the present work. Moreover, little ligninolytic activity was observed during the colonization of wood, i.e., no reduction in the intensity of the aromatic signals. In addition, the relative intensity of the 1640 cm^{-1} band increased, which would indicate the increase of conjugated ketone group, observed also in brown-rot and non-selective white-rot [16]. The FTIR spectra showed as well the increase, although to a lesser extent, of the 1427 cm^{-1} and 1375 cm^{-1} bands, which Xu and coworkers have assigned to lignin monomer vibrations and C-H bending of cellulose and hemicellulose. The latter increase could be explained by the overlapping of C-H bending vibrations of hemicelluloses and fungal polysaccharides present in the heart rot [42,43,48]. The intensity of the aromatic C-O stretching signal at 1244 cm^{-1} increased in the same manner as the 1427 cm^{-1} band, further proving the increase in lignin/polyphenolic substance in the heart rot samples. Contrary to the fungal brown rot decay, no decrease in the carbohydrate bands were observed, including the anomeric signals at 898, 830, and 805 cm^{-1}, except for the disappearance of the shoulder at around 985 cm^{-1}. This band could be assigned to pectic polymers and hemicelluloses such as arabinogalactan or xyloglucan [12,13]. Since there is no clear reduction in the intensity of carbohydrates or lignin, it could be concluded that *I. obliquus* simultaneously decays the two polymers. The disappearance of the 985 and 1730 cm^{-1} bands suggested that *I. obliquus* has a slight preference for the degradation of hemicelluloses and pectic compounds.

To the best of our knowledge, this was the first time ^{13}C CP-MAS NMR spectroscopy has been applied to the study of birch wood decay caused by *I. obliquus*. As reported in Table 1, the application of the lignin methoxyl content calibration curve obtained by Evstigneyev and coworkers [34] to our spectroscopic data indicated a decrease in the methyl content of lignin in the heart rot of birch. Lignin demethylation and hemicellulose degradation would be in agreement with the soft rot classification [5]. While, in the ^{13}C CPMAS NMR spectra, the total carbon in the 5–45 ppm range increased from sapwood to heart rot (Table 1), the intensity of the acetyl group decreased (Fig. 1). The increase of the aliphatic carbon could be ascribed to the deposition of suberin as a defense mechanism as it has been observed already in birch infected by *I. obliquus* [49]. On the other hand, the amount of carbonyl ^{13}C increased from sapwood to heart rot, although with high deviation. Nevertheless, some differences were observed: the sapwood lacked the 143 ppm peak (free hydroxyl position of the aromatic unit, Table 2) and the shoulder around 178 ppm (COOH, Section 3.1). The lack of the 143 ppm peak is interesting, because it suggested the absence of demethylated lignin or of polyphenolic compounds with free hydroxyl groups (such as lignans). The increase in the carboxylic carbon could be due to the synthesis of phenolic acids or similar molecules by the birch tissues. On the other hand, both brown- and white-rot decay have been shown to produce oxalic acid to degrade hemicelluloses and oxalate salts have been observed in sections of colonized wood [5]. These spectroscopical findings indicate that the classification of *I. obliquus* as white-rot fungus might not be adequate and its genomics should be investigated in more detail. The most recent genome analysis of this fungus gave little insight on this aspect [50], besides suggesting high carbohydrate degradation capacity, which would be in agreement with the hemicellulose degradation observed in our study.

4. Conclusions

Solid state ^{13}C NMR and FTIR spectroscopies have been applied for the first time to study the sterile conk of *I. obliquus* (Chaga). Sterile conk samples were compared to cultivated *I. obliquus* and birch heart rot caused by this fungus. The application of principal component analysis to the obtained datasets demonstrated that the sterile conk formation model of Biggs can be applied to *Inonotus obliquus*: the fungal tissue was concentrated below the black bark and hyphae spread in the birch wood towards the periderm. The black bark resulted, compared to the brown-yellow layers below, spectroscopically more similar to wood tissues. The similarity of the layers below the bark to both decayed wood and hyphae was shown by the multivariate data analysis of both spectra datasets and the use of the spectral distance algorithm. The spectra collected from the heart rot showed lack of lignin degradation, except for demethoxylation, and the slight preference for hemicellulose degradation, suggesting that the classification of *I. obliquus* as white-rot fungus should be revised by further studies.

Declaration of Competing Interest

The authors declare that they have no known competing financial interests or personal relationships that could have appeared to influence the work reported in this paper.

CRediT authorship contribution statement

Gabriele Beltrame: Conceptualization, Methodology, Software, Formal analysis, Investigation, Writing – original draft, Writing – review & editing, Visualization, Funding acquisition. **Ida Mattsson:** Methodology, Investigation, Writing – review & editing. **Pia Damlin:** Conceptualization, Methodology, Writing – original draft,

Supplementary materials

Supplementary material associated with this article can be found, in the online version, at doi:10.1016/j.molstruc.2022.133226.

References

[1] U. Grienke, M. Zöll, U. Peintner, J.M. Rollinger, European medicinal polypores - a modern view on traditional uses, J. Ethnopharmacol. 154 (2014) 564–583, doi:10.1016/j.jep.2014.04.030.

[2] A.P. Singh, T. Singh, Biotechnological applications of wood-rotting fungi: a review, Biomass Bioenergy 62 (2014) 198–206, doi:10.1016/j.biombioe.2013.12.013.

[3] T. Manavalan, A. Manavalan, K. Heese, Characterization of lignocellulolytic enzymes from white-rot fungi, Curr. Microbiol. 70 (2015) 485–498, doi:10.1007/s00284-014-0743-0.

[4] G. Daniel, Fungal degradation of wood cell walls, in: Second. Xylem Biol., Elsevier, 2016, pp. 131–167. 10.1016/B978-0-12-802185-9.00008-5.

[5] F.W.M.R. Schwarze, Wood decay under the microscope. Fungal Biol. Rev. 21 (2007) 133–170, doi:10.1016/j.fbr.2007.09.001.

[6] M.E. Balandaykin, I.V. Zmitrovich, Review on chaga medicinal mushroom, Inonotus obliquus (Higher Basidiomycetes): realm of medicinal applications and approaches on estimating its resource potential, Int. J. Med. Mushrooms. 17 (2015) 95–104, doi:10.1615/IntJMedMushrooms.v17.i2.10.

[7] M. Saar, Fungi in khanty folk medicine, J. Ethnopharmacol. 31 (1991) 175–179, doi:10.1016/0378-8741(91)90003-V.

[8] Y. Zhao, W. Zheng, Deciphering the antitumoral potential of the bioactive metabolites from medicinal mushroom Inonotus obliquus, J. Ethnopharmacol. 265 (2021) 113321, doi:10.1016/j.jep.2020.113321.

[9] A.L. Shigo, How poria obliqua and polyporus glomeratus incite canker, Phytopathology 59 (1969) 1164–1165.

[10] R. Blanchette, R. Biggs, Defense Mechanisms of Woody Plants Against Fungi, Springer Berlin Heidelberg, Berlin, Heidelberg, 1992, doi:10.1007/978-3-662-01642-8.

[11] R.A. Blanchette, Progressive stages of discoloration and decay associated with the canker-rot fungus, Inonotus obliquus, in Birch, Phytopathology 72 (1982) 1272–1277.

[12] M. Chylińska, M. Szymańska-Chargot, A. Zdunek, FT-IR and FT-Raman characterization of non-cellulosic polysaccharides fractions isolated from plant cell wall, Carbohydr. Polym. 154 (2016) 48–54, doi:10.1016/j.carbpol.2016.07.121.

[13] M. Kacuráková, P. Capek, V. Sasinková, N. Wellner, A. Ebringerová, FT-IR study of plant cell wall model compounds: pectic polysaccharides and hemicelluloses, Carbohydr. Polym. 43 (2000) 195–203, doi:10.1016/S0144-8617(00)00151-X.

[14] F.J. Warren, M.J. Gidley, B.M. Flanagan, Infrared spectroscopy as a tool to characterise starch ordered structure - A joint FTIR-ATR, NMR, XRD and DSC study, Carbohydr. Polym. 139 (2016) 35–42, doi:10.1016/j.carbpol.2015.11.066.

[15] M.K. Jang, B.G. Kong, Y. Il Jeong, C.H. Lee, J.W. Nah, Physicochemical characterization of α-chitin, β-chitin, and γ-chitin separated from natural resources, J. Polym. Sci. Part A Polym. Chem. 42 (2004) 3423–3432, doi:10.1002/pola.20176.

[16] K... Pandey, A. Pitman, FTIR studies of the changes in wood chemistry following decay by brown-rot and white-rot fungi, Int. Biodeterior. Biodegradation. 52 (2003) 151–160, doi:10.1016/S0964-8305(03)00052-0.

[17] I. Santoni, E. Callone, A. Sandak, J. Sandak, S. Dirè, Solid state NMR and IR characterization of wood polymer structure in relation to tree provenance, Carbohydr. Polym. 117 (2015) 710–721, doi:10.1016/j.carbpol.2014.10.057.

[18] F. Peter-Valence, C. Llarena-Hernandez, M. Largeteau, J.M. Savoie, F. Ruaudel, F. Ziarelli, E. Ferré, A.M. Farnet, Chemical characterization of the biomass of an edible medicinal mushroom, agaricus subrufescens, via solid-state 13C NMR, J. Agric. Food Chem. 59 (2011) 8939–8943, doi:10.1021/jf2017622.

[19] M.F. Davis, H.A. Schroeder, G.E. Maciel, Solid-state 13c nuclear magnetic resonance studies' of wood decay, Holzforschung 48 (1994) 186–192, doi:10.1515/hfsg.1994.48.3.186.

[20] C.H. Vane, T.C. Drage, C.E. Snape, Bark decay by the white-rot fungus Lentinula edodes: polysaccharide loss, lignin resistance and the unmasking of suberin, Int. Biodeterior. Biodegrad. 57 (2006) 14–23, doi:10.1016/j.ibiod.2005.10.004.

[21] H. Chen, C. Ferrari, M. Angiuli, J. Yao, C. Raspi, E. Bramanti, Qualitative and quantitative analysis of wood samples by Fourier transform infrared spectroscopy and multivariate analysis, Carbohydr. Polym. 82 (2010) 772–778, doi:10.1016/j.carbpol.2010.05.052.

[22] J. Lehto, J. Louhelainen, T. Kłosińska, M. Drożdżek, R. Alén, Characterization of alkali-extracted wood by FTIR-ATR spectroscopy, Biomass Convers. Biorefinery. 8 (2018) 847–855, doi:10.1007/s13399-018-0327-5.

[23] G.K. Gomba, A. Synytsya, P. Švecová, M.A. Coimbra, J. Čopíková, Distinction of fungal polysaccharides by N/C ratio and mid infrared spectroscopy, Int. J. Biol. Macromol. 80 (2015) 271–281, doi:10.1016/j.ijbiomac.2015.05.059.

[24] H. Sivonen, M. Nuopponen, S.L. Maunu, F. Sundholm, T. Vuorinen, Carbon-thirteen cross-polarization magic angle spinning nuclear magnetic resonance and Fourier transform infrared studies of thermally modified wood exposed to brown and soft rot fungi, Appl. Spectrosc. 57 (2003) 266–273, doi:10.1366/000370203321558164.

[25] G. Mollica, F. Ziarelli, S. Lack, F. Brunel, S. Viel, Characterization of insoluble calcium alginates by solid-state NMR, Carbohydr. Polym. 87 (2012) 383–391, doi:10.1016/j.carbpol.2011.07.066.

[26] P. Strunk, T. Öman, A. Gorzsás, M. Hedenström, B. Eliasson, Characterization of dissolving pulp by multivariate data analysis of FT-IR and NMR spectra, Nord. Pulp Pap. Res. J. 26 (2011) 398–409.

[27] J. Miina, R. Peltola, P. Veteli, R. Linnakoski, M.C. Escribano, J. Haveri-Heikkilä, P. Mattila, P. Marnila, J.M. Pihlava, J. Hellström, T. Sarjala, N. Silvan, M. Kurttila, H. Vanhanen, Inoculation success of Inonotus obliquus in living birch (Betula spp.), For. Ecol. Manag. 492 (2021) 119244, doi:10.1016/j.foreco.2021.119244.

[28] K.H. Ka, S.M. Jeon, H. Park, B.H. Lee, S.R. Ryu, Growth of chaga mushroom (Inonotus obliquus) on betula platyphylla var. japonica, Korean J. Mycol 45 (2017) 241–245, doi:10.4489/KJM.20170029.

[29] C.W. Wold, C. Kjeldsen, A. Corthay, F. Rise, B.E. Christensen, J.Ø. Duus, K.T. Inngjerdingen, Structural characterization of bioactive heteropolysaccharides from the medicinal fungus Inonotus obliquus (Chaga), Carbohydr. Polym. 185 (2018) 27–40, doi:10.1016/j.carbpol.2017.12.041.

[30] G. Beltrame, J. Trygg, J. Hemming, Z. Han, B. Yang, Comparison of polysaccharides extracted from cultivated mycelium of Inonotus obliquus with polysaccharide fractions obtained from sterile conk (Chaga) and birch heart rot, J. Fungi 7 (2021) 189, doi:10.3390/jof7030189.

[31] G. Beltrame, J. Hemming, H. Yang, Z. Han, B. Yang, Effects of supplementation of sea buckthorn press cake on mycelium growth and polysaccharides of Inonotus obliquus in submerged cultivation, J. Appl. Microbiol. 131 (2021) 1318–1330, doi:10.1111/jam.15028.

[32] R. Studio, R. Studio, Integrated Development for R, RStudio, Inc., Boston, MA, 2020 URL http://www.rstudio.com/.

[33] H. Wikberg, S.L. Maunu, Characterisation of thermally modified hard- and softwoods by C CPMAS NMR, Carbohydr. Polym. 58 (4) (2004) 461–466, doi:10.1016/j.carbpol.2004.08.008.

[34] E.I. Evstigneyev, A.S. Mazur, A.V. Kalugina, A.V. Pranovich, A.V. Vasilyev, Solid-state 13 C CP/MAS NMR for Alkyl-O-Aryl bond determination in lignin preparations, J. Wood Chem. Technol. 38 (2018) 137–148, doi:10.1080/02773813.2017.1393436.

[35] A. Synytsya, M. Novák, Structural diversity of fungal glucans, Carbohydr. Polym. 92 (2013) 792–809, doi:10.1016/j.carbpol.2012.09.077.

[36] A.C. Ruthes, F.R. Smiderle, M. Iacomini, Mushroom heteropolysaccharides: a review on their sources, structure and biological effects, Carbohydr. Polym. 136 (2016) 358–375, doi:10.1016/j.carbpol.2015.08.061.

[37] P. Jandura, B.V. Kokta, B. Riedl, Fibrous long-chain organic acid cellulose esters and their characterization by diffuse reflectance FTIR spectroscopy, solid-state CP/MAS ¹³C-NMR, and X-ray diffraction, J. Appl. Polym. Sci. 78 (7) (2000) 1354–1365, doi:10.1002/1097-4628(20001114)78:7⟨1354::AID-APP60⟩3.0.CO;2-V.

[38] J. Jung, I. Lee, S. Seok, H. Lee, Y. Kim, B. Yun, Antioxidant polyphenols from the mycelial culture of the medicinal fungi Inonotus xeranticus and Phellinus linteus, J. Appl. Microbiol. 104 (2008) 1824–1832, doi:10.1111/j.1365-2672.2008.03737.x.

[39] I.K. Lee, Y.S. Kim, Y.W. Jang, J.Y. Jung, B.S. Yun, New antioxidant polyphenols from the medicinal mushroom Inonotus obliquus, Bioorganic Med. Chem. Lett. 17 (2007) 6678–6681, doi:10.1016/j.bmcl.2007.10.072.

[40] W. Zheng, K. Miao, Y. Liu, Y. Zhao, M. Zhang, S. Pan, Y. Dai, Chemical diversity of biologically active metabolites in the sclerotia of Inonotus obliquus and submerged culture strategies for up-regulating their production, Appl. Microbiol. Biotechnol. 87 (2010) 1237–1254, doi:10.1007/s00253-010-2682-4.

[41] I.K. Lee, B.S. Yun, Styrylpyrone-class compounds from medicinal fungi phellinus and Inonotus spp., and their medicinal importance, J. Antibiot. 64 (2011) 349–359 Tokyo, doi:10.1038/ja.2011.2.

[42] V. Mohaček-Grošev, R. Božac, G.J. Puppels, Vibrational spectroscopic characterization of wild growing mushrooms and toadstools, Spectrochim. Acta Part A Mol. Biomol. Spectrosc. 57 (2001) 2815–2829, doi:10.1016/S1386-1425(01)00584-4.

[43] A. Synytsya, M. Novak, Structural analysis of glucans, Ann. Transl. Med. 2 (2014) 17, doi:10.3978/j.issn.2305-5839.2014.02.07.

[44] Y. Nakajima, Y. Sato, T. Konishi, Antioxidant small phenolic ingredients in Inonotus obliquus (persoon) pilat (Chaga), Chem. Pharm. Bull. 55 (2007) 1222–1226, doi:10.1248/cpb.55.1222.

[45] J. Kim, S.C. Yang, A.Y. Hwang, H. Cho, K.T. Hwang, Composition of triterpenoids in Inonotus obliquus and their anti-proliferative activity on cancer cell lines, Molecules 25 (2020) 4066, doi:10.3390/molecules25184066.

[46] X. Xu, Z. Xu, S. Shi, M. Lin, Lignocellulose degradation patterns, structural changes, and enzyme secretion by Inonotus obliquus on straw biomass under submerged fermentation, Bioresour. Technol. 241 (2017) 415–423, doi:10.1016/j.biortech.2017.05.087.

[47] L. Xiao, Z. Shi, Y. Bai, W. Wei, X.-.M. Zhang, S. Run-Cang, Biodegradation of lignocellulose by white-rot fungi: structural characterization of water-soluble hemicelluloses, (2013). 10.1007/s12155-013-9302-y.

[48] N. Dalonso, G.H. Goldman, R.M.M. Gern, β-(1→3),(1→6)-Glucans: medicinal activities, characterization, biosynthesis and new horizons, Appl. Microbiol. Biotechnol (2015), doi:10.1007/s00253-015-6849-x.

[49] M.M. Rahman, F. Ishiguri, Y. Takashima, M.A.K. Azad, K. Iizuka, N. Yoshizawa, S. Yokota, Anatomical and histochemical characteristics of Japanese birch (Tohoku) plantlets infected with the Inonotus obliquus IO-U1 strain, Plant Biotechnol. 25 (2008) 183–189, doi:10.5511/plantbiotechnology.25.183.

[50] Y. Duan, H. Han, J. Qi, J. Gao, Z. Xu, P. Wang, J. Zhang, C. Liu, Genome sequencing of Inonotus obliquus reveals insights into candidate genes involved in secondary metabolite biosynthesis, BMC Genom. 23 (2022) 1–17, doi:10.1186/s12864-022-08511-x.